



# 3D MULTIMODEL BRAIN TUMOR IMAGE CLASSIFICATION AND SEGMENTATION USING DEEP LEARNING

Mrs.P.Gokila, M.E<sup>1</sup>., Mrs.P.Sundari, M.E<sup>2</sup>.,

Aathifa Nusrath.S<sup>3</sup>, Aishwarya.J<sup>4</sup>, Gowtham.S<sup>5</sup>, Manoj.M<sup>6</sup>

Assistant Professor- CSE, Info Institute of Engineering Coimbatore<sup>1</sup>

Assistant Professor- IT, Info Institute of Engineering Coimbatore<sup>2</sup>

( UG Scholars )Info Institute of Engineering Coimbatore<sup>3-6</sup>

**Abstract:** Brain tumor segmentation from 3D images is one of the most important and challenging tasks in the field of medical imaging. Manual classification can lead to false predictions and diagnoses. Moreover, this is a difficult process when the supporting data is enormous.. Extracting brain tumour regions from MRI images becomes challenging due to the great variety of appearances of brain tumours and how similar they are to normal tissues. In this article, we designed a modified U-Net architecture under a deep learning framework for brain real images for medical imaging and computer-assisted interventions provided by the BRATS2020 dataset. Test accuracy of 99.4% has been achieved. A comparative review with other papers shows our model using U-Net performs better than other deep learning-based models.

**Keywords:** Deep learning, brain tumor classification and segmentation, 3d unet architecture.

## INTRODUCTION

Medical image processing is a technique and method for generating a visual depiction of the body's inside, as well as a function of some organ or tissue, for clinical research and medical treatment. Medical imaging is designed to highlight hidden internal structures for disease detection and treatment.. Medical imaging also generates a database of regular anatomical structures and physiology to aid in the detection of anomalies. Medical image processing refers to the manipulation of images using a computer. This process involves various types of techniques and operations, such as retrieving, saving, displaying, and communication images. This process facilitates the detection and treatment of incidents and the identification of abnormalities by following a database of normal organ structure and function. It includes both organic and CT imaging using MRI, magnetism, oscilloscope, thermal, and isotope imaging. There are many other strategies for recording data regarding body position and function. These techniques have many limitations compared to the engine that creates the image. One of the image processing techniques is using a computer to manipulate digital images. This technique has many advantages such as resilience, adaptability, data storage, and communication. As various image resizing technologies grow, you can save images efficiently. This technique has many rule sets for running images synchronously.

The brain can have many different types of abnormalities, the most likely of which is a brain tumor. Brain tumors occur due to abnormal cell growth in the brain. The brain's structure is extremely complicated, where several regions are in charge of various nervous system activities. Tumors can form anywhere in the brain or skull, including the protective linings, the base of the brain, and other regions. There are different kinds of brain tumors that exist and they depend on what tissue they arise from. Each year, tens of thousands of individuals are diagnosed with brain tumors., deep learning algorithms have sparked interest in the automated diagnosis and categorization of brain tumors. These techniques have also been used for segmentation of brain tumors, and the medical community has paid much attention to this area. The purpose of segmentation is to change how various portions of an image are represented, making it easier to interpret areas of the image with distinct properties. After the brain image is divided into these many different sections, each region is spatially contiguous.. The lengthy-time requirements and the possibility of misclassification due to the problem's complexity are two prominent challenges in the manual identification of brain tumors. As a result, automated segmentation of brain MRI images can greatly improve diagnostic and therapeutic procedures, especially when access to radiologists and qualified specialists is limited. Many research studies can be found related to x-ray or CT images but works on MRI image segmentation are comparatively less. MRI images are difficult to manipulate because they are highly hardware dependent, and they have one or more additional dimensions that distinguish them from typical RGB



images. Each image can very well be bigger than 1GB. The computation and space required for training large MRI datasets are very high. Each year, thousands of people around the world are diagnosed with brain tumors. This has sparked interest in the field of automated diagnosis and categorization of brain tumors using deep learning algorithms. The main purpose of segmentation is to change the representation of image segments to make it easier to interpret regions of the image with different properties. Each area becomes spatially contiguous after separating the picture of the brain into distinct sections. This lengthy time requirement and the possibility of misclassification due to the problem of complexity are two prominent challenges in the identification of manual detection of brain tumors. Hence, automatic segmentation of 3D MRI images of the brain can greatly improve diagnosis and treatment procedures, especially when access to qualified medical experts and radiologists is limited. Inspired by UNet which is designed for handling medical images we have used it here for brain tumor segmentation using 3D MRI images.

## METHODS AND MATERIALS

### EXPLORING AND VISUALIZING THE DATASET:

The image dataset used in this work is the Brats2020 dataset containing 3D MRI in 'nii' format. In order to properly visualize the dataset and understand the images to perform further operations, several neural imaging libraries such as "nilearn" and "nibabel" were used. These libraries were used to load the "nii" images and plot the images in different forms. Given below is a visual representation of an MRI image. MRI images of different settings.

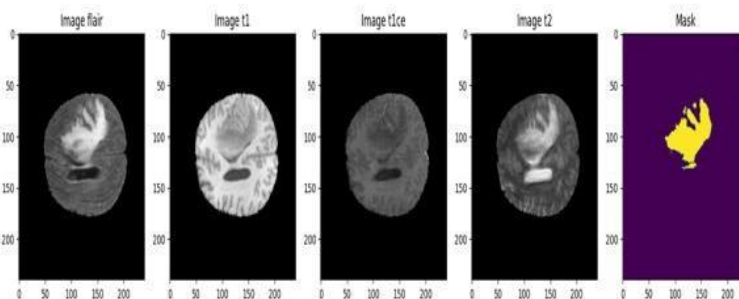


FIGURE 1: VISUAL REPRESENTATION OF AN MRI IMAGE

## MODEL ARCHITECTURE

**U-Net Architecture:** U-Net developed by Ronneberger et al. is an architecture for semantic segmentation which uses a Fully Convolution Network Model. The purpose of semantic image segmentation is to give each and every pixel in a picture a class that symbolizes something. This task is usually known as a dense prediction because we're predicting each pixel in the image. U-Net is popularly used in medical image segmentation. A radiologist's analysis can be complemented by a device that uses U-Net. This significantly reduces the time it takes to perform diagnostic procedures.

The contracting path and the expanding path together make up the model. The reducing/contracting path follows the typical architecture of a convolutional network which downsamples an image. It is made up of two  $3 \times 3$  convolutions that are applied repeatedly (unpadded convolutions), with a rectified linear unit (ReLU) coming after each for down-sampling, a  $2 \times 2$  max pooling operation with stride 2 is used. Each stage in the downsampling process doubles the number of feature channels. In each stage of the expansive path, the feature map is up-sampled, followed by a  $2 \times 2$  convolution ("up-convolution") that cuts the number of feature channels in half, a concatenation with the proportionally cropped feature map from the contracting path, and a ReLU following each of the two  $3 \times 3$  convolutions. Cropping is essential since every convolution results in the loss of border pixels. The final layer uses  $1 \times 1$  convolution to split each 64-component feature vector into a related number of classes. The given network contains an aggregate of 23 convolutional layers. In the final layer, Softmax has been used as activation. Given in figure is the U-net

### ALGORITHM:

Proposed 3D UNet Model

Step 1: Normalising and resizing the BraTS dataset images.

Step 2: This is the encoder part, we use standard convolutions and a max-pooling unit ( $2 \times 2$ ) in each level, and the depth of the image slowly increases while the image size gradually reduces, starting from  $128 \times 128 \times 2$  to  $8 \times 8 \times 512$ .



- I. CONV2D 1: output:  $128 \times 128 \times 32$ ,  
kernel size:  $3 \times 3$ , activation function: 'ReLU';
- II. MAX\_POOLING2D: output:  $64 \times 64 \times 32$ , pool size:  $2 \times 2$ ;
- III. CONV2D 2: output:  $64 \times 64 \times 64$ , kernel size:  $3 \times 3$ , activation function: 'ReLU';
- IV. CONV2D 3: output:  $64 \times 64 \times 64$ , kernel size:  $3 \times 3$ , activation function: 'ReLU';
- V. MAX\_POOLING2D: output:  $32 \times 32 \times 64$ , pool size:  $2 \times 2$ ;
- VI. CONV2D 4: output:  $32 \times 32 \times 128$ , kernel size:  $3 \times 3$ , activation function: 'ReLU'; model architecture that was used in this paper. As a loss function, the categorical cross-entropy was used here equ. 1 as the loss function which is popularly used in multi-class classification tasks.
- VII. CONV2D 5: output:  $32 \times 32 \times 128$ , kernel size:  $3 \times 3$ , activation function: 'ReLU';
- VIII. MAX\_POOLING2D: output:  $16 \times 16 \times 128$ , pool size:  $2 \times 2$ ;
- IX. CONV2D 6: output:  $16 \times 16 \times 256$ , kernel size:  $3 \times 3$ , activation function: 'ReLU';
- X. CONV2D 7: output:  $32 \times 32 \times 256$ ,  
kernel size:  $3 \times 3$ , activation function: 'ReLU';
- XI. MAX\_POOLING2D: output:  $8 \times 8 \times 256$ , pool size:  $2 \times 2$ ;
- XII. CONV2D 8: output:  $8 \times 8 \times 512$ , kernel size:  $3 \times 3$ , activation function: 'ReLU';
- XIII. CONV2D 9: output:  $8 \times 8 \times 512$ , kernel size:  $3 \times 3$ , activation function: 'ReLU';

Step 3: Then, in the decoder, we used transposed convolutions along with standard convolutions to gradually expand the image size while reducing the depth, from  $8 \times 8 \times 512$  to  $128 \times 128 \times 2$ .

- I. DROPOUT
- II. UP\_SAMPLING\_2D: output:  $16 \times 16 \times 512$ , kernel size:  $2 \times 2$ , activation function: 'ReLU';
- III. CONV2D 10: output:  $16 \times 16 \times 256$ , kernel size:  $3 \times 3$ , activation function: 'ReLU';
- IV. CONCATENATE 1: output:  $16 \times 16 \times 512$ ;
- V. CONV2D 11: output:  $16 \times 16 \times 256$ ,  
kernel size:  $3 \times 3$ , activation function: 'ReLU';
- VI. CONV2D 12: output:  $16 \times 16 \times 256$ , kernel size:  $3 \times 3$ , activation function: 'ReLU';
- VII. UP\_SAMPLING\_2D: output:  $32 \times 32 \times 256$ , kernel size:  $2 \times 2$ , activation function: 'ReLU';
- VIII. CONV2D 13: output:  $32 \times 32 \times 128$ , kernel size:  $3 \times 3$ , activation function: 'ReLU';
- IX. CONCATENATE 2: output:  $32 \times 32 \times 256$ ;
- X. CONV2D 14: output:  $32 \times 32 \times 128$ ,  
kernel size:  $3 \times 3$ , activation function: 'ReLU';
- XI. CONV2D 15: output:  $32 \times 32 \times 128$ , kernel size:  $3 \times 3$ , activation function: 'ReLU';
- XII. UP\_SAMPLING\_2D: output:  $64 \times 64 \times 128$ , kernel size:  $2 \times 2$ , activation function: 'ReLU';
- XIII. CONV2D 16: output:  $64 \times 64 \times 128$ , kernel size:  $3 \times 3$ , activation function: 'ReLU';
- XIV. CONCATENATE 3: output:  $64 \times 64 \times 128$ ;
- XV. CONV2D 17: output:  $64 \times 64 \times 64$ , kernel size:  $3 \times 3$ , activation function: 'ReLU';
- XVI. CONV2D 18: output:  $64 \times 64 \times 64$ , kernel size:  $3 \times 3$ , activation function: 'ReLU';
- XVII. UP\_SAMPLING\_2D: output:  $128 \times 128 \times 64$ , kernel size:  $2 \times 2$ , activation function: 'ReLU';
- XVIII. CONV2D 19: output:  $128 \times 128 \times 32$ , kernel size:  $3 \times 3$ , activation function: 'ReLU';
- XIX. CONCATENATE 4: output:  $128 \times 128 \times 64$ ;
- XX. CONV2D 20: output:  $128 \times 128 \times 32$ , kernel size:  $3 \times 3$ , activation function: 'ReLU';
- XXI. CONV2D 19: output:  $128 \times 128 \times 32$ , kernel size:  $3 \times 3$ , activation function: 'ReLU';
- XXII. CONV2D 19: output:  $128 \times 128 \times 4$ , kernel size:  $3 \times 3$ , activation function: 'Softmax';

Step 4: The encoder part's layers are skip connected and are concatenated with the decoder part's layers (those are mentioned as gray lines in the above diagram), due to which the U-Nets to generate an image in the decoder part using fine-grained details learned in the encoder part. Step 5: Finally, the loss function and model were set up. Our optimizer is Adam, and the loss function used here is Categorical Cross-Entropy Loss.

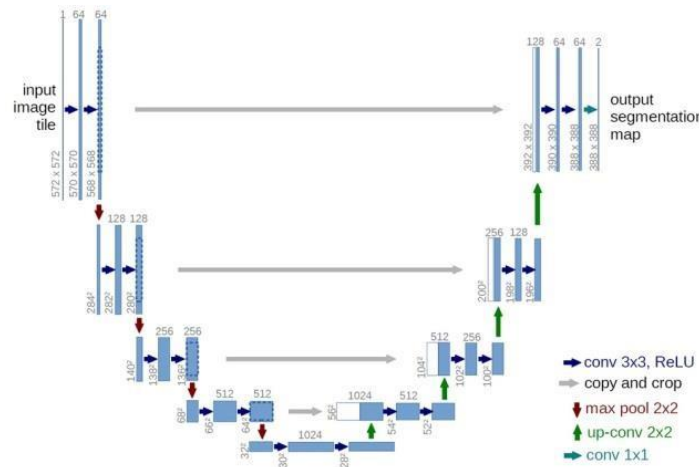


FIGURE 2: U-NET ARCHITECTURE

**MODEL TRAINING:**

Initially the model was trained with 15 epochs, but the nature of the graphs showed gradual improvement, then in order to get better results the number of epochs was increased to 25 where the results were better but in order to reinforce our results further it was increased to 35 epochs where the results were getting stabilized. Finally, the model was trained with 35 epochs and it took 12 hours for the training process to be complete so that it be used further the model was saved in an h5 file named “model\_x1\_1.h5”. When training the model, I saved all the metrics for each epoch. Then the saved model was loaded and used to plot metrics for training and validation. In Figure, the graphs show the training metrics where the blue line symbolizes the training metric and the red line describes the validation metric, where the y-axis indicates the number of epochs and the x-axis indicates the score. Figure shows the accuracy of training and validation with varying epochs. It states that training accuracy is slightly higher than validation accuracy and they reach the plateau at about 20 epochs. Figure shows training and validation loss, and the difference is about 0.01 so it can be concluded that it is a good fit. Figure 3 shows a significant increase in dice with a subsequent increase in the number of epochs in both training and validation. Finally Figure 3 shows that the dice increased significantly and the number of epochs increased for both training and validation. The mean IoU score of training and validation reached a value greater than 0.5 after about 15 epochs, and greater than 0.8 after about 25 epochs which is a good score to have.

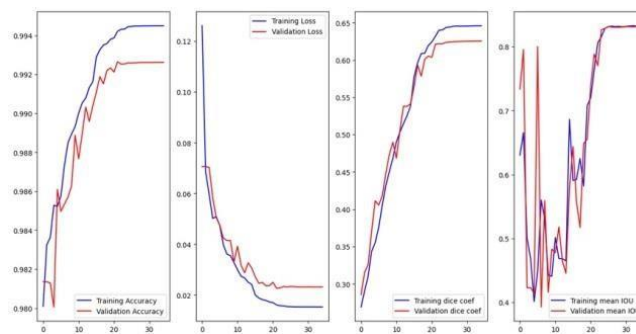


FIGURE 3: VALIDATION AND TRAINING ACCURACY

**PREDICTIONS:**

For predicting the presence of tumor in the brain and classifying its classes the model was trained and used, then the original MRI image along with the ground truth images and the prediction classes were plotted for proper visualization of the predictions. In the predictions below Random Images were taken in order to visualize how accurately the algorithm is predicting. Figures 4, which are images of the brain containing the tumor, show that our predictions are in good agreement with the ground truth.

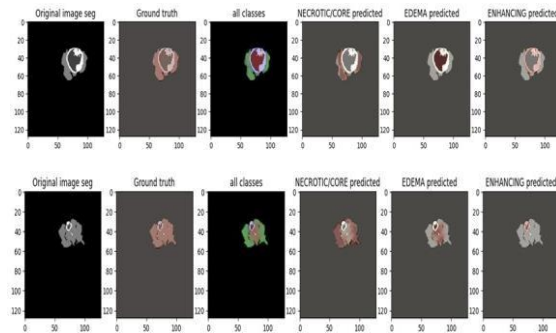


FIGURE 4: PREDICTIONS

it is observed that the ground truth image and the predictions from left to right where (a) is the original image, (b) is the ground truth image, (c) shows all the tumor classification, (d) is the prediction for Necrotic/Core region, (e) is the prediction for Edema region and finally (f) is the Enhancing region.

#### EVALUATION METRICS :

The model was evaluated to generate different metrics using the test data by using a data generator to randomize the data, and the batch size taken was 100. The following metrics were obtained and are shown in Table 1 below: precision [39], loss, cubic coefficient, mean IOU, precision, sensitivity, and specificity. The saved model was used to evaluate the given metrics to create a scorecard where these metrics are shown for both training set and validation set.

#### COMPARATIVE ANALYSIS:

In order to represent how much improvement U-Net Architecture provides compared to some other popular methods of brain tumor detection can be clearly seen by doing a comparative study, where we take the same dataset and find out the metrics for other algorithms. below shows a tabular representation of the comparative analysis.

#### RESULTS:

The dataset used here was MICCAI BRATS 2020 Dataset contains 371 training files which was taken from Kaggle. The model was trained on Kaggle with the specifications 2-core of Intel Xeon as CPU, Tesla P100 16GB VRAM as GPU, with 13GB RAM. In the training process, 35 epochs were run to train this model which took us about 14 hours to train. The task of identifying tumors is very difficult. The position, form, and structure of tumors differ greatly from one patient to the next, making segmentation a difficult process. In figure, various scans of the same brain sliced segment from different patients, clearly indicate the tumor diversity. The position of the tumor is obviously different in each of the eight images/patients presented. In reality, Figure 5 shows the tumor can be divided into many regions .

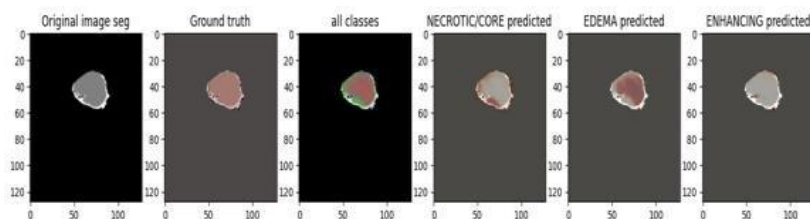


FIGURE 5: TUMOR DIVIDED REGIONS

#### DISCUSSION: PROBLEM DEFINITION:

Segmentation of gliomas in pre-operative MRI scans. Each pixel on image must be labeled: Pixel is part of tumor region (1 or 2 or 3) -> can be one of several classes/sub-regions All others -> pixel is not on tumor region (0) for evaluation The sub-regions of tumors considered for are:

1) 'enhanced tumor' (ET), 2) 'tumor core' (TC), and 3) 'whole tumor' (WT) The segmentation labels provided are , has the value 1 for NCR and NET, and 2 for ED. 4 for ET, 0 otherwise.

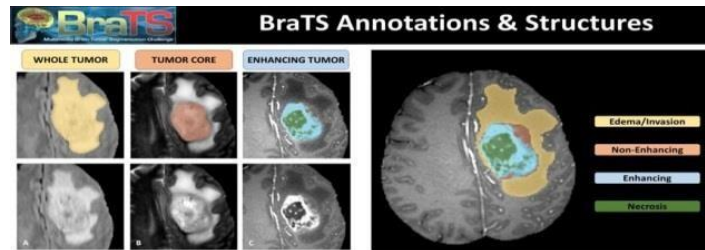


FIGURE 6:LEVELS OF TUMOR

### IMAGE DATA DESCRIPTION:

All BraTS multimodal scans are available as NIFTI files (.nii.gz) -> commonly used to store brain image data acquired on MRI and describe various MRI settings. Medical image format used T1: T1-weighted, native image, sagittal or axial 2D image with slice thickness 1-6 mm. T1c: T1-weighted, contrast-enhanced (gadolinium) imaging, 3D acquisition, 1 mm isotropic voxel size for most patients. T2: T2-weighted image, 2D axial acquisition, slice thickness 2-6 mm. FLAIR: T2-weighted FLAIR images, 2D axial, coronal or sagittal views, 2-6 mm slice thickness. Data were collected from multiple (n = 19) institutions using different clinical protocols and different scanners. All image datasets were manually segmented by one of his four raters using the same annotation protocol, and their annotations were approved by an experienced neuroradiologist. Annotations included GD-enhanced tumors (ET - label 4), peritumoral edema (ED - label 2), and necrotic and non-enhanced tumor cores (NCR/NET - label 1), both in BraTS 2012-It is listed. 2013 TMI paper and latest BraTS abstract paper.

Data were acquired with different clinical protocols and various scanners from multiple (n=19) institutions.

All the imaging datasets have been segmented manually, by one to four raters, following the same annotation protocol, and their annotations were approved by experienced neuro-radiologists. Annotations comprise the GD-enhancing tumor (ET — label 4), the peritumoral edema (ED — label 2), and the necrotic and non-enhancing tumor core (NCR/NET — label 1), as described both in the BraTS 2012-2013 TMI paper and in the latest BraTS summarizing paper. The provided data are distributed after their pre-processing, i.e., co-registered to the same anatomical template, interpolated to the same resolution (1 mm<sup>3</sup>) and skull-stripped.

### METHODOLOGY

The main research methodology that has been used is classification research in which the brain tumor is going to be classification and comparative research where the obtained classification will be compared with other classifications in order to study the improvements obtained. In order to train the model, 3D MRI images have been needed. The data for this paper was collected from the BRATS2020 dataset which was available publicly. The dataset was already grouped into images for training and testing. Then the tumor regions were defined in the high-resolution 3D MRI images by using U-Net Model to downsample the images into a lower resolution in order to identify the features more efficiently, this part is also known as the encoder path. And then again the images are upsampled with the preserved extracted feature also known as the decoder path. It is used to find and distinguish boundaries by performing a classification on each pixel so that the input and output are the same size, resulting in the input and output having the same size. So in the downsampling or encoder path, our model gets to know “WHAT” is present in the image and in the upsampling or decoder path the model recovers the “WHERE” information (or where it is present in the image).

### DATASET DESCRIPTION:

This paper uses the BRATS2020 dataset because a dataset containing many MRI images is required to perform this task. Multimodal scans of the BraTS dataset are available as NIFTI files (.nii.gz). It is a medical imaging format commonly used to store brain image data acquired with MRI and to describe various MRI settings. T1-weighted, native images, sagittal or axial 2D slices 1-6 mm thick. T1c: T1-weighted, contrast-enhanced (gadolinium) image with her 3D acquisition and isotropic voxel size of 1 mm for most patients. T2-weighted image, 2D axial acquisition, slice thickness 2-6 mm. T2-weighted FLAIR images, axial, coronal or sagittal 2D images, slice thickness 2–6 mm [21]. Data were collected from multiple (n=19) centers using different clinical protocols and different scanners. All image datasets were manually segmented by 1–4 raters



using the same annotation technique, and the annotations were reviewed and validated by an expert neuroradiologist. Annotations include peritumoral edema (ED - label 2), GD-enhanced tumor (ET - label 4), and necrotic and non-enhanced tumor core (NCR/NET - label 1). Both of these are described in BraTS 2012-. His TMI paper from 2013 and his latest BraTS overview of that paper. After preprocessing, the data are distributed. This includes mutual registration to the same anatomical template, interpolation to the original resolution (1mm<sup>3</sup>), and skull stripping.

#### ACKNOWLEDGEMENTS:

We would like to express our gratitude to the following individuals and organizations for their contributions to this study: Our team members for their dedication and hard work throughout the project BraTS multimodal scans are available as NIfTI files (.nii.gz). Dataset collected by Kaggle .

The cloud computing provider that enabled us to leverage its infrastructure for efficient training of our deep learning models.

The open-source software communities that provided us with various tools and libraries for data processing, analysis, and visualization.

The funding agencies that supported this research and enabled us to conduct this study.

We are also grateful to the anonymous reviewers for their constructive feedback and suggestions that helped us to improve the quality and clarity of our manuscript.

Finally, we would like to acknowledge all the patients who participated in this study and made this research possible.

#### APPENDIX:

##### A. HYPER PARAMETERS FOR DEEP LEARNING MODELS:

TABLE A.1: HYPERPARAMETERS FOR 3DUNET ARCHITECTURE:

Hyperparameter	Value/method
Layers	3 encoding, 3 decoding
# Epochs	500
# Convolutional filters in the first layer	24
Convolutional kernel size	3
Max pooling kernel size	3
Stride kernel size	2
Weight initialization	He <i>et al</i> (2015)
Optimizer	Adam (Kingma and Ba 2015) with default parameters
Learning rate	$1 \times 10^{-3}$
Loss function	Weighted cross entropy
Batch size	1
Dropout	0.5

##### B. CODE AVAILABILITY:

The source code for the deep learning models and the data preprocessing pipeline used in this study are available on GitHub at

<https://github.com/IBM-EPBL/IBM-Project-4274-1658727164.git>



C.SUPPLEMENTARYFIGURES:

BRAIN VOLUME SETTINGIMAGE:

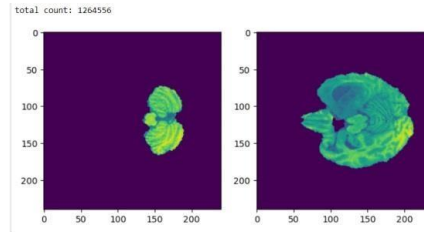


FIGURE 7: BRAIN VOLUME SETTING.

3D FLIP IMAGES:

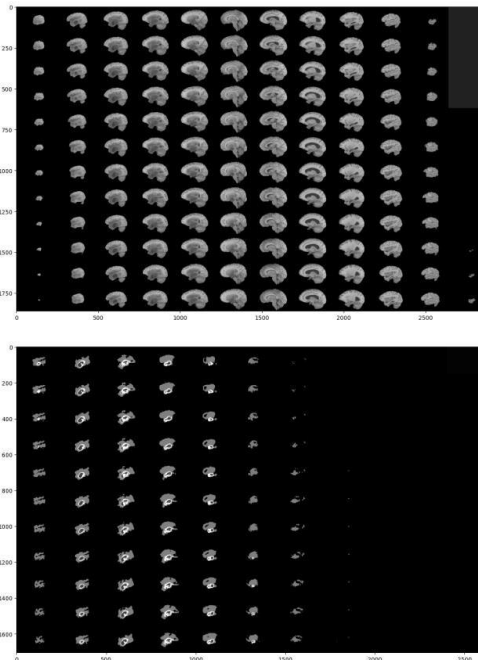


FIGURE 8: 3D FLIP IMAGES.

IMAGE SEGMENTATION:

1. Annotation image:

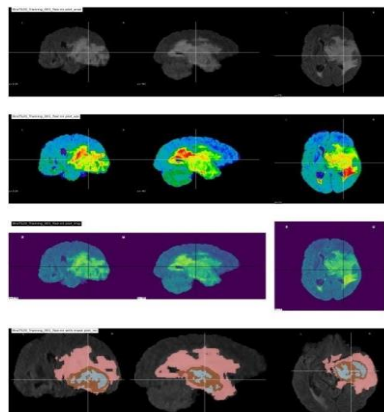


FIGURE 9 : IMAGE SEGMENTATION





2. EPI Image. 3.Normal Mask Image.4.Region of Intersect.  
these are the four level of images inthis image segmentation.

OUTPUT IMAGE:

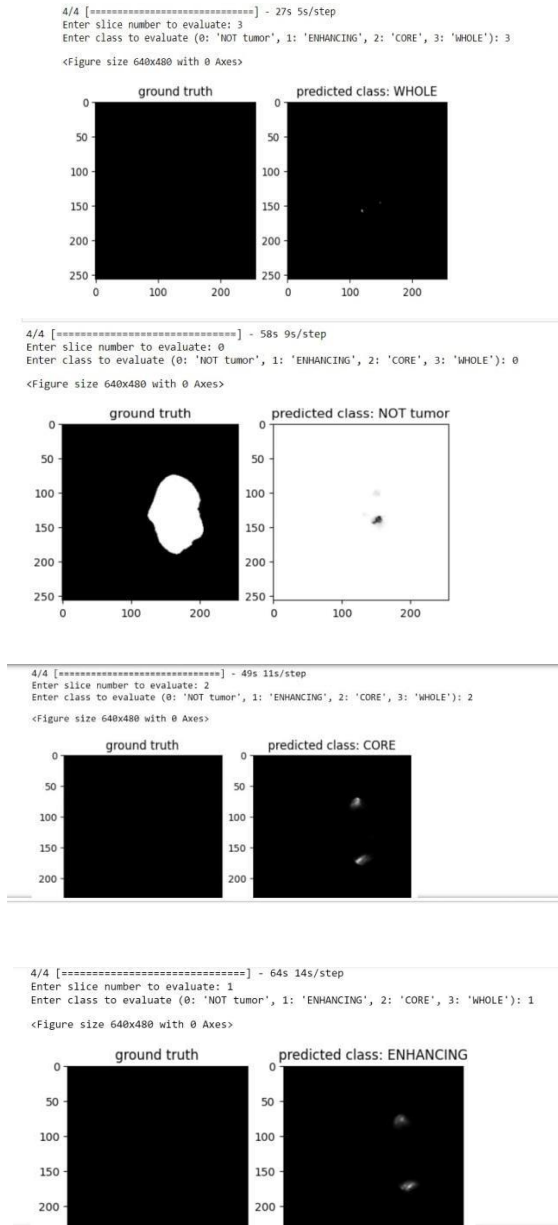


FIGURE 10:OUTPUT IMAGES.

FORMULAS:

DICE COEFFICIENT:

$$\text{loss} = ((2. * \text{intersection} + \text{smooth}) / (K.\text{sum}(y\_true\_f) + K.\text{sum}(y\_pred\_f) + \text{smooth}))$$

$$\text{total\_loss} = \text{total\_loss} / \text{class\_num}$$

PRECISION:

$$\text{Precision} = \text{true\_positives} / (\text{predicted\_positives} + K.\text{epsilon}())$$



**BLOCK DIAGRAM:**

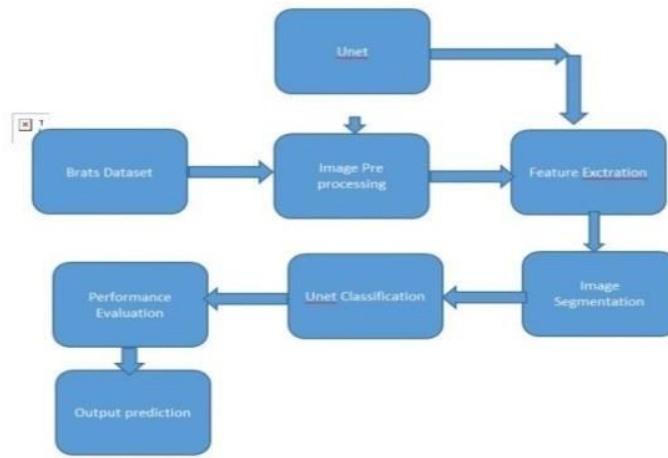


FIGURE 11:3D UNET ARCHITECTUREBLOCK DIAGRAM

After collecting the BRATS dataset, wepreprocessed the images and performed segmentation according to different classessuch as no tumor, edema, necrosis/nucleus and enhanced tumor. Additionally, feature extraction was performed on tumors during training and classified accordingly. Finally, the model predicted outputs based on the results and was saved for futureevaluation and comparative analysis runs. The process flow diagram in Figure 2 shows the path of the thesimplimentation from start to finish.

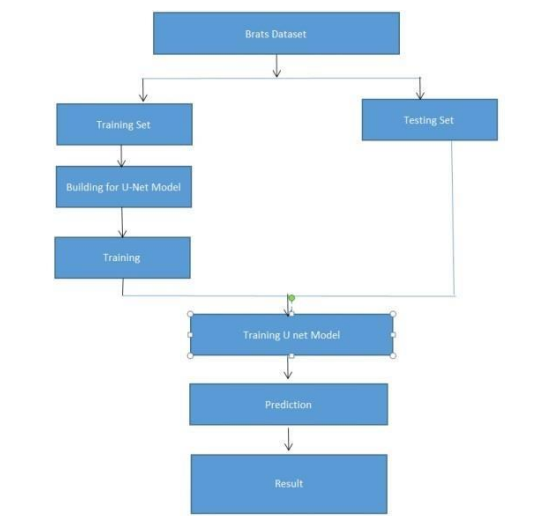


FIGURE 12:OVERALL PROCESSBLOCK DIAGRAM

**CONCLUSION**

The main goal of this research is focused on developing automatic segmentation of medical images. H. Rapid detection of tumors in the brain. In medical imaging, assisted segmentation by radiologists has proven to be very time-consuming and resource-intensive, and may not be available in remote locations. Therefore, this task of highly automated techniques for detecting brain tumors proves to be of great benefit in a considerable number of cases.To overcome this obstacle, the main algorithm used in this paper is a U-Net thathelps delineate tumors, is very close to the ground truth, and also made very accurate predictions on MRI images. This articledescribes different methods for progressiveand innovative detection of brain tumors. The first preprocessed segment used the median filtering technique to preprocess the MRI images and achieved 99% validation accuracy performed on the BRATS2020 dataset. As a result, target regions are segmented and the approachprovided herein can be used to determine the presence of tumors, allowing physicians to plan treatment and monitor tumors throughout the diagnostic period. The advantage of this approach is that it improves the level of image



segmentation and its spatial localization, thus providing superior performance compared to other systems. It trains faster and takes less time to compute than other networks with fewer parameters. Further research includes improving accuracy with low error rates by using different classifier algorithms. Moreover, it can be modified and used to predict survival in brain tumor patients. Future work may include the use of larger and more diverse datasets useful for testing in real-world scenarios and clinical trials.

## REFERENCES

- [1] Ahuja S, Panigrahi BK, Gandhi T (2020). "Transfer Learning Based Brain Tumour Detection and Segmentation using Superpixel Technique," 2020 International Conference on Contemporary Computing and Applications (IC3A), 2020, pp. 244-249 .
- [2] Tripathi P, Singh VK, Trivedi MC (2021). "Brain tumor segmentation in magnetic resonance imaging using OKM approach", Materials Today: Proceedings, Volume 37, Pages 1334-1340.
- [3] Miglani A, Madan H, Kumar S, Kumar S (2021). "A Literature Review on Brain Tumour Detection and Segmentation," 2021 5th International Conference on Intelligent Computing and Control Systems (ICICCS), pp. 1513-1519.
- [4] Cherguif H, Riffi J, Mahraz, M A, Yahyaouy A, Tairi A (2019). "Brain Tumour Segmentation Based on Deep Learning," 2019 International Conference on Intelligent Systems and Advanced Computing Sciences (ISACS), pp. 1-8.
- [5] Mesut T, Zafer C, Burhan E, (2020). "Classification of Brain MRI Using Hyper Column Technique with Convolutional Neural Network and Feature Selection Method". Expert Systems with Applications. 149.
- [6] Choudhury CL, Mahanty C, Kumar R, Mishra BK, (2020). "Brain Tumour Detection and Classification Using Convolutional Neural Network and Deep Neural Network," 2020 International Conference on Computer Science, Engineering and Applications (ICCSEA), pp. 1-4.
- [7] Thias AH, Al Mubarak AF, Handayani A, Danudirdjo D, Rajab TE, (2019). "Brain Tumor Semi-automatic Segmentation on MRI T1- weighted Images using Active Contour Models," 2019 International Conference on Mechatronics, Robotics and Systems Engineering (MoRSE), pp. 217-221.
- [8] Çinar A, Yildirim M, (2020). "Detection of tumors on brain MRI images using the hybrid convolutional neural network architecture", Med. Hypotheses, vol. 139, p. 109684.
- [9] Abdelaziz Ismael SA, Mohammed A, Hefny H (2020). "An enhanced deep learning approach for brain cancer MRI images classification using residual networks". Artif Intell Med.
- [10] Badža MM., Marko CB (2020). "Classification of Brain Tumors from MRI Images Using a Convolutional Neural Network" Applied Sciences 10.
- [11] Afshar P, Mohammadi A, Plataniotis KN, (2020). "BayesCap: A Bayesian Approach to Brain Tumour Classification Using Capsule Networks," in IEEE Signal Processing Letters, vol. 27, pp. 2024-2028.